JOURNAL OF CHEMICAL INFORMATION AND MODELING

Article

pubs.acs.org/jcim

Development of a Comprehensive, Validated Pharmacophore Hypothesis for Anthrax Toxin Lethal Factor (LF) Inhibitors Using Genetic Algorithms, Pareto Scoring, and Structural Biology

Ting-Lan Chiu and Elizabeth A. Amin*

Department of Medicinal Chemistry and Minnesota Supercomputing Institute for Advanced Computational Research, University of Minnesota, 717 Delaware St. SE, Minneapolis, Minnesota 55414-2959

Supporting Information

ABSTRACT: Anthrax is an acute infectious disease caused by the spore-forming bacterium *Bacillus anthracis*. The anthrax toxin lethal factor (LF), an 89-kDa zinc hydrolase secreted by the bacilli, is the toxin component chiefly responsible for pathogenesis and has been a popular target for rational and structure-based drug design. Although hundreds of small-molecule compounds have been designed to target the LF active site, relatively few reported inhibitors have exhibited activity in cell-based assays, and no LF inhibitor is currently available to treat or prevent anthrax. This study presents a new pharmacophore map assembly, validated by experiment, designed to rapidly identify and prioritize promising LF inhibitor scaffolds from virtual compound libraries. The new hypothesis incorporates structural information from all five available LF enzyme−inhibitor complexes deposited in the Protein Data Bank (PDB) and is the first LF pharmacophore map reported to date that includes features representing interactions involving all three key subsites of the LF catalytic binding region. In a wide-ranging validation study on all 546 compounds for which published LF biological activity data exist, this model displayed strong selectivity toward nanomolar-level LF inhibitors, successfully identifying 72.1% of existing nanomolar-level compounds in an unbiased test set, while rejecting 100% of weakly active (>100 μM) compounds. In addition to its capabilities as a database searching tool, this comprehensive model points to a number of key design principles and previously unidentified ligand−receptor interactions that are likely to influence compound potency.

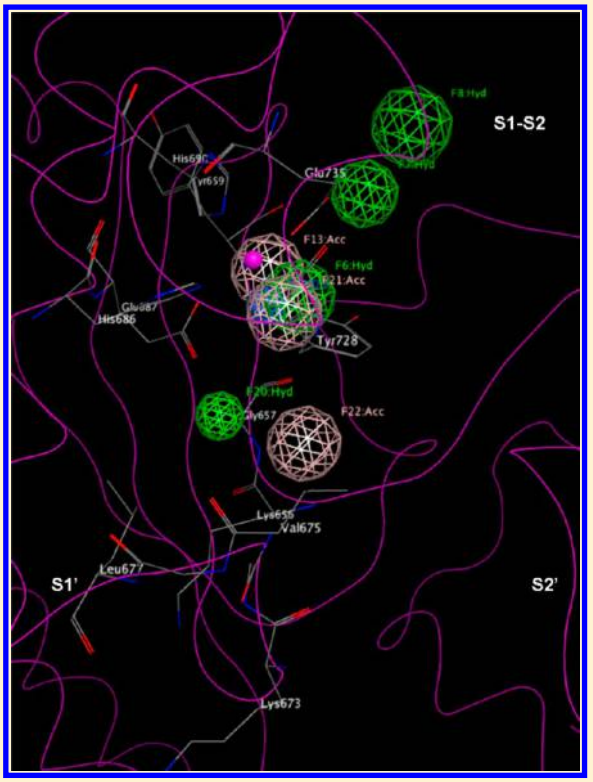

INTRODUCTION

The rod-shaped, spore-forming bacterium *Bacillus anthracis* has emerged as one of the most dangerous biological weapons. As the causative agent of anthrax, the bacillus secretes a tripartite exotoxin comprising the lethal factor (LF), edema factor adenylate cyclase (EF), and protective antigen (PA), encoded by the pXO1 plasmid.[1] The LF enzyme, a zinc metalloprotein, is the primary agent of anthrax-related toxicity. LF joins with PA to form the anthrax lethal toxin,[2] which enters cells and cleaves members of the mitogen activated protein kinase kinase (MAPKK) family, interfering with cellular immune defense mechanisms and allowing the pathogen to replicate unchecked.[3−6] Host death may result suddenly from massive release of cytokines from spore-infected macrophages or in later stages of the disease from circulatory shock due to vascular barrier disruption and hypovolemia.[7−10] The anthrax bacilli are susceptible to antibiotics, but early diagnosis and treatment are essential, as antibacterial therapeutics have no effect on the rapidly secreted lethal toxin. In cases of inhalational anthrax, host death is certain without treatment, and mortality rates approach 50% even with prophylactic antibiotics and aggressive support including mechanical ventilation, fluids, and vasopressors.[11−13]

As anthrax continues to pose a significant biowarfare threat, new and more effective treatment modalities are in high demand, and small-molecule LF inhibitors have attracted particular attention as potential postexposure drugs to be administered in the aftermath of a bioterror attack.[6,9,14−35] LF inhibitor design is nontrivial, however, because of the presence of a catalytic zinc, challenging active-site topology, and cross-reactivity resulting from relatively high sequence homology

Received: March 6, 2012
Published: June 14, 2012

dx.doi.org/10.1021/ci300121p | J. Chem. Inf. Model. 2012, 52, 1886−1897

with other zinc metalloproteins at the catalytic center.[9,28,36−41] LF inhibitor scaffolds have progressed from small peptide sequences designed as substrate mimics[10,36,42] to nonpeptidic acids incorporating hydroxamate groups,[9] which are especially strong zinc chelators, to small molecules featuring a variety of other zinc-binding groups (ZBGs) intended to avoid the pharmacokinetic liabilities associated with hydroxamates,[15,16,24−26,32,34,43−54] yet no LF inhibitor has yet made it to the market as a preventive or therapeutic agent.

LF is a 90-kDa Zn metalloprotein consisting of four domains (Figure 1). The C-terminal domain includes the LF active site,

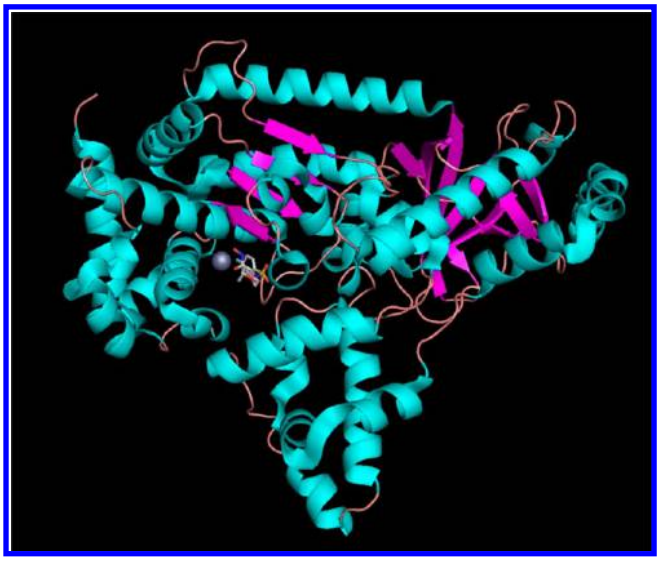

Figure 1. Anthrax toxin lethal factor domains II−IV (residues 297−809) (1YQY.pdb[55]), colored by secondary structure, with catalytic Zn^{2+} (gray sphere) and cocrystallized hydroxamate inhibitor **MK-702**/**LF-1B** (visualized in MacPyMOL 1.5.0.1, Schrödinger, LLC).

in which a catalytic Zn^{2+} is coordinated to three active-site residues: His686, His690, and Glu735, all located on α-helices and comprising part of the signature HEXXH consensus sequence found in many Zn metalloproteinases.[9,43] Three subsites comprise the LF substrate binding region: the hydrophobic and sterically restricted S1′ subsite, the less constrained and partly solvent-exposed S1−S2 region, and the less well-characterized, open-ended S2′ area (Figure 2).

Many diverse compound classes have been designed to inhibit LF; examples include small peptide sequences designed to parallel the natural MAPKK substrate with hydroxamic acid ZBGs,[10,36,42] sulfonamide hydroxamate compounds,[9] rhodanines,[16,25,26,43] and N,N′-diquinoline urea derivatives,[46] among others. Overall, hundreds of small-molecule LF inhibitors have been reported in the literature,[6,9,14−35] and five X-ray structures of LF-ligand complexes are available in the Protein Data Bank (PDB): 1YQY,[55] 1ZXV,[16] 1PWP,[46] 1PWU,[36] and 1PWQ.[36] Cocrystallized inhibitors in these structures include the most active LF inhibitor designed to date, a sulfonamide hydroxamate (IC_{50} = 0.054 μM,[9] 1YQY), a rhodanine derivative (IC_{50} = 1.7 μM,[24] 1ZXV), a *N,N′*-diquinoline urea analog (K_i = 0.5 μM,[46] 1PWP), and two peptide hydroxamates (K_i^{app} = 2.1 μM[36] and 11 μM,[36] 1PWQ and 1PWU, respectively). Figure 3 illustrates a superposition of all five ligands on the basis of alignment of X-ray receptor structures (MOE 2010.10, Chemical Computing Group, Inc.). The chemical functionalities of these five ligands occupy various key regions of the LF

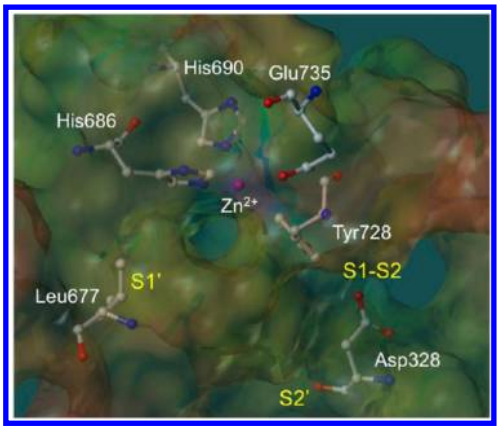

Figure 2. Active site of the anthrax toxin lethal factor (1YQY.pdb[55]), with MOLCAD electrostatic potential mapping (red = positive, purple = negative); catalytic Zn^{2+} (magenta sphere); zinc-binding residues His686, His690, and Glu735; and illustrating three binding subsites: S1′, S1−S2, and S2′,[56] visualized in SYBYL 8.0., Tripos, Inc.

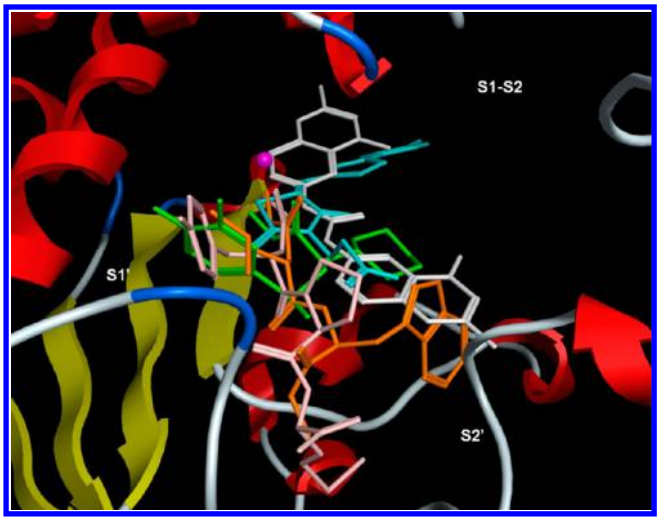

Figure 3. Superposition of bound conformations of five active anthrax toxin LF inhibitors[9] obtained via protein alignment (MOE 2010.10) illustrating the three binding subsites (visualized in MOE 2011.10). White = **NSC 12155**;[46] orange = **GM6001**;[36] green = **MK-702**/**LF-1B**;[55] cyan = **BI-MFM3**;[16] pink = thioacetyl-Tyr-Pro-Met-amide.[36]

active site and taken together cover all three critical subsites (S1′, S1−S2, S2′) of the LF binding area.

Researchers are actively seeking novel LF inhibitor scaffolds[23,29,35,56] that demonstrate favorable biological activities, explore new regions in chemical space, and serve as starting points for antianthrax drug design. Pharmacophore mapping has long been recognized as a valuable computational tool to pinpoint new drug and probe scaffolds based on ligand−receptor interactions engaged in by active compounds.[57−59] LF inhibitor pharmacophore hypotheses have been reported in the literature and recommended for database screening.[35,46,54,60] However, these models were developed from limited training sets, i.e., from one or two structural classes of compounds found to partly occupy the LF binding site, which somewhat restricts their applicability and usefulness as searching tools. In the current study, we report a comprehensive pharmacophore model, **UM1**, which is designed to overcome this roadblock by building on experimentally determined binding modes involving the entire LF binding area. This new model was

dx.doi.org/10.1021/ci300121p | J. Chem. Inf. Model. 2012, 52, 1886−1897

generated from a series of five preliminary maps **UA1−5** using genetic algorithms,[61] Pareto scoring,[62,63] and ligand−receptor interaction diagrams based on experimental structural biology. The final model was validated using a data set comprising 546 LF inhibitors—**all** compounds known to date with published in vitro biological activities against LF—including an unbiased external test set of 68 nanomolar-level LF inhibitors that are structurally dissimilar to the compounds used to construct and optimize the model. We show that when implemented with a partial match criterion of at least five features, all of which passed a key statistical significance test, **UM1** successfully identified 49 (72.1%) of the 68 most potent LF inhibitors (IC_{50} or K_i < 1 μM) in the unbiased test set, and rejected all compounds with specified IC_{50} or K_i values greater than 100 μM. In addition to its highly selective searching ability, this comprehensive map elucidates important design principles for highly potent LF inhibitors. Specifically, a small molecule effective against LF must incorporate at least five of the following eight features: (1−3) three hydrophobic groups to interact with hydrophobic sidechains in the S1−S2 and zinc-chelating regions of the active site; (4) a hydrogen-bond acceptor interacting with Glu687 near the catalytic zinc; (5) hydrophobic interactions with one or more of the following: Lys656 (S2′), Leu677 (S1′), His686 (catalytic zinc area), or Tyr728 (S1-S2); (6) a hydrogen-bond acceptor interacting with Glu735 (S1-S2) or Tyr728; (7) a hydrogen-bond acceptor interacting with Lys656 or Gly657 (at the S2′ entrance); or (8) a hydrogen-bond donor interacting with Gly657 and/or Glu687.

RESULTS AND DISCUSSION

Preliminary Pharmacophore Models. Five initial pharmacophore maps **UA1−5** were generated on the basis of the aforementioned experimental X-ray structures deposited in the Protein Data Bank.[64] Two of these models, **UA1** and **UA2**, were derived from active LF inhibitor series using genetic algorithms (GAs) and a scoring function based on Pareto multiobjective optimization, as implemented in the GALAHAD package[61] (Tripos, Inc.). One model (**UA3**) was generated by modifying a published pharmacophore map based on further examination of ligand−receptor interactions observed in LF X-ray structures. Models **UA4** and **UA5** were obtained by creating new pharmacophoric feature representations derived solely from crystallographic enzyme−inhibitor interactions, as no analogs or derivatives of cocrystallized ligands from those complexes have been made available. Both GA-based hypotheses contained data from all molecules in the input set and were represented as a set of hypermolecules (ligand alignments and common features such as hydrogen bond donors/acceptors and hydrophobic centers). The GA models were subjected to multiple iterative refinements, and their accuracy was assessed by means of two key criteria: an overall Pareto score and a rank sum value incorporating (a) pharmacophoric concordance (a measure of the overall pharmacophoric similarity among ligand conformers), (b) steric overlap (a measure of the overall steric similarity among ligand conformers), and (c) agreement between the query tuplet and the pharmacophoric tuplets for the ligands as a group (essentially, a measure of similarity between the pharmacophoric query and the compound set used to build the model).[61,65] Within each set of hypotheses, models were ranked first by Pareto score; if all Pareto scores were equal, the models were then ordered by the rank sum value across criteria (a−c) listed above. Any remaining "ties" were subsequently broken by a total energy term representing the energies of all molecules in the training set (as estimated by the Tripos force field), where lower energies are considered more favorable.[61,65] It is important to note that the presence of a given feature and/or chemical functionality in more than one active compound does not necessarily indicate a significant contribution to compound activity or signify a true enzyme−inhibitor interaction. We therefore generated two-dimensional ligand−receptor interaction maps (MOE 2010.10, Chemical Computing Group, Inc.) for each cocrystallized complex to eliminate those features in each hypothesis that either did not parallel enzyme−inhibitor interactions as observed in the X-ray structures or that represented those interactions inaccurately (i.e., incorrect hydrogen bonding directionality). As the MOE-based 2D maps do not illustrate hydrophobic interactions, we also generated PoseView[66] 2D diagrams to clarify those interactions in three cases (models **UA3−5**).

*Model **UA1**: 1YQY.pdb (LF Cocrystallized with the Sulfonamide Hydroxamate MK-702/LF-1B[55]).* Fifteen preliminary hypotheses were derived from the five most active compounds in ref 9, as determined by LF FRET assay IC_{50} values: **38**, **39**, **46**, **49**, and **50** (Table 1), with in vitro activities

Table 1. Five Most Active Sulfonamide Hydroxamate LF Inhibitor Compounds from Ref 9, As Determined by in Vitro LF FRET Assay IC_{50} Values

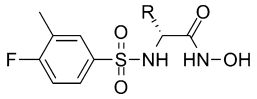

Cpd #	R	LF IC_{50} (μM)
38	*c*-Hex	0.042
39	Ph	0.050
46	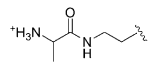	0.037
49	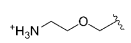	0.048
50	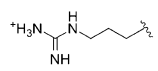	0.040

ranging from 0.037 to 0.050 μM. All 15 models exhibited an equivalent Pareto rank, so the six-featured hypothesis UA1_001 was chosen from among these by overall rank sum across pharmacophoric concordance, steric overlap, and tuplet agreement criteria as described earlier. On the basis of ligand−receptor interaction diagrams of the 1YQY.pdb X-ray structure (Figure 4a,b), two alterations were made to UA1_001: a feature representing the sulfonamide NH moiety as an acceptor was removed, and the hydroxamate ZBG hydroxyl was represented as a hydrogen-bond donor. The resulting final model **UA1** is shown in Figure 4c.

*Model **UA2**: 1ZXV.pdb (LF Bound to **BI-MFM3**, a Rhodanine Derivative).* Twenty preliminary models were derived from the three most active compounds **6**, **7** and **8** (with in vitro LF FRET assay activities from 0.19 to 0.30 μM) in ref 24 (Table 2); all 20 hypotheses once again exhibited identical Pareto scores. The most favorable model chosen by

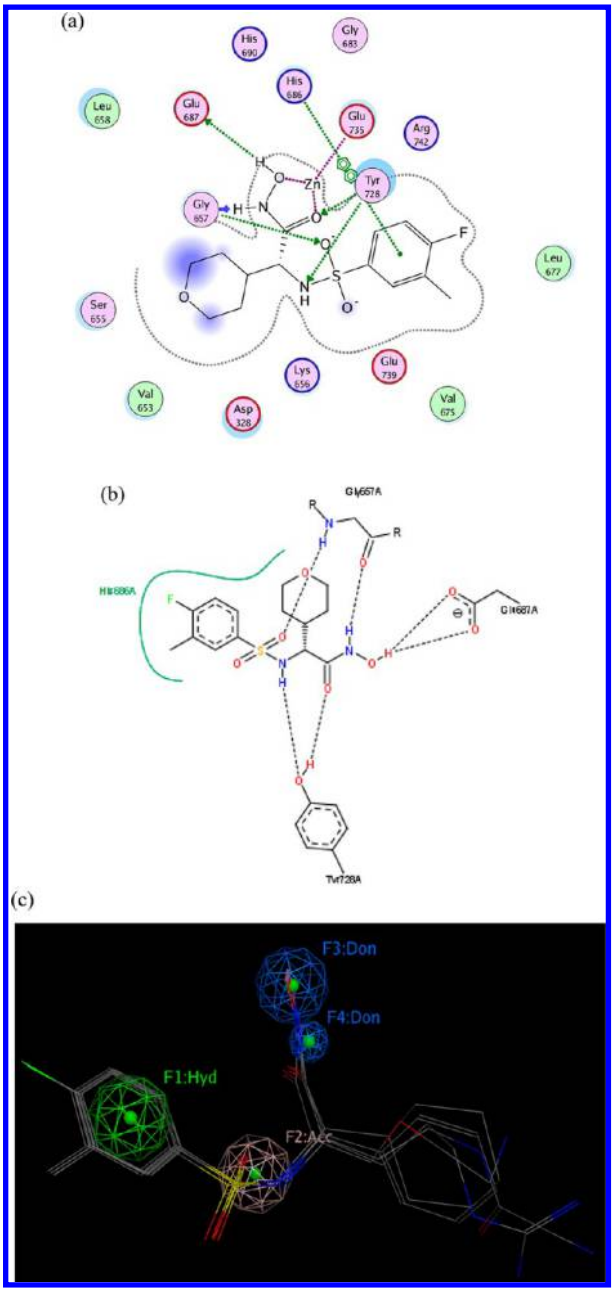

Figure 4. (a) Ligand−receptor interaction diagram of sulfonamide hydroxamate **MK-702** (**LF-1B**, **40**) cocrystallized with the anthrax toxin lethal factor (1YQY.pdb[55]) (MOE 2010.10, Chemical Computing Group, Inc.). In this and subsequent MOE interaction diagrams, green spheres = "greasy" residues; spheres with red outline = acidic residues; spheres with blue outline = basic residues; spheres with black outline = polar residues; blue background spheres = receptor exposure to solvent; blue spheres on ligand atoms = ligand exposure to solvent; green dotted lines = side chain donors/acceptors; blue dotted lines = backbone donors/acceptors; purple dotted line = metal contact; gray dotted line = proximity contour. (b) Additional ligand−receptor interaction map of **MK-702** (**LF-1B**, **40**) bound to LF (1YQY.pdb[55]) (PoseViewWeb[66]); in this and subsequent PoseView interaction diagrams, dashed lines = directed bonds between protein and ligand; spline sections = hydrophobic contacts between ligand moieties and the indicated receptor residues. (c) Preliminary LF inhibitor pharmacophore model **UA1** based on a series of highly active analogs of **MK-702**;[9] green sphere = hydrophobic features; blue spheres = hydrogen-bond donors; pink sphere = hydrogen-bond acceptor (visualized in MOE 2010.10).

Table 2. Three Most Active Rhodanine-Based LF Inhibitor Compounds from Ref 24, As Determined by in Vitro LF FRET Assay IC_{50} Values

Cpd #	Structure	LF IC_{50} (μM)
6	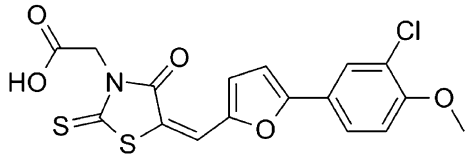	0.30
7	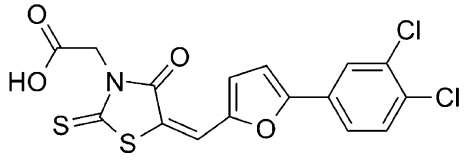	0.26
8	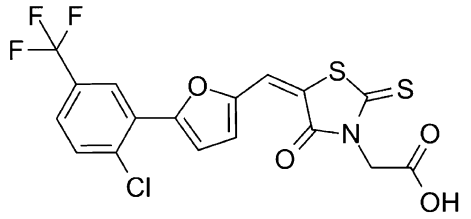	0.19

pharmacophoric rank sum value, UA2_001, initially comprised six features. The ligand−receptor interaction diagrams for 1ZXV.pdb (Figure 5a,b) did not illustrate any ligand moieties functioning as hydrogen-bond acceptors; therefore, two such features in UA2_001, corresponding to a furan oxygen and a carboxylic acid oxygen on the ligands, were removed. Additionally, a fast Connolly electron density surface of the LF active site including **BI-MFM3** was generated with lipophilic potential mapping using MOLCAD[67] in SYBYL 8.0 (Tripos, Inc.) (Figure 5c). This surface points to hydrophobic regions in the LF Zn-chelating and S1−S2 areas comprising Val653, Leu658, Tyr659, Pro661, and Tyr728, supporting the inclusion of three hydrophobic features corresponding to phenyl, furan, and 2-thioxothiazolidine-4-one moieties on the ligand that interact with this receptor area. An anionic feature in UA2_001 was also retained, as it corresponds to a solvent-exposed carboxylic acid functionality on the ligand set. The revised, final hypothesis **UA2** comprised four features in total and is depicted in Figure 5d.

*Model **UA3**: 1PWP.pdb (LF Complexed with **NSC 12155**, a Methylquinoline Urea Derivative).* Previously, Panchal and coworkers[46] had developed a partial pharmacophore model of the LF S1-S2 subsite on the basis of inhibitors **NSC 12155**, compound **1** (K_i = 0.5 μM) and **NSC 357756**, compound **2** (K_i = 4.9 μM) (Table 3). The initial hypotheses were refined by those workers using six other active compounds from virtual and experimental NCI database screening to generate the final reported model.[46] This five-featured hypothesis comprised two aromatic centers, two polar centers, and one neutral linker. However, only two aromatic features in this published model were present in experimental interaction diagrams of the 1PWP complex (Figure 6a,b), so the other three features were deleted to form revised model **UA3** (Figure 6c).

dx.doi.org/10.1021/ci300121p | J. Chem. Inf. Model. 2012, 52, 1886−1897

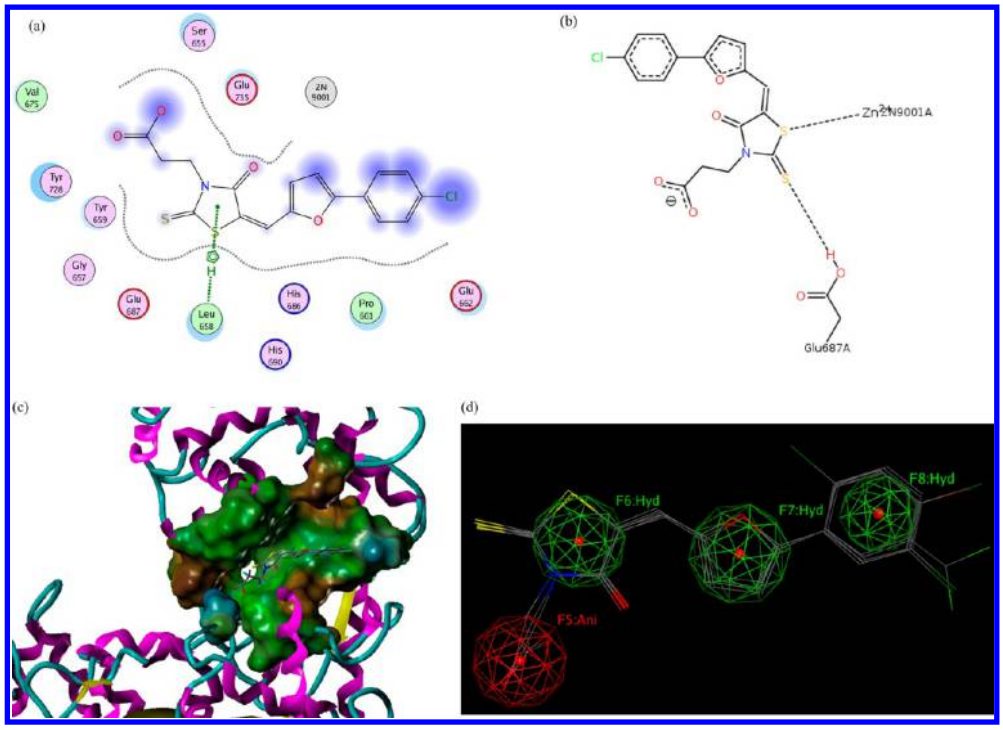

Figure 5. (a) Ligand–receptor interaction diagram of rhodanine derivative **BI-MFM3** cocrystallized with the anthrax toxin lethal factor (1ZXV.pdb[16]) (MOE 2010.10). (b) Additional ligand–receptor interaction map of **BI-MFM3** bound to LF (1ZXV.pdb[16]) (PoseViewWeb [66]). (c) MOLCAD Fast Connolly electron density surface of the LF active site (1ZXV.pdb[16]) with lipophilic potential mapping, shown with **BI-MFM3**; brown = highest lipophilicity; blue = highest hydrophobicity (SYBYL 8.0, Tripos, Inc.). (d) Preliminary LF inhibitor pharmacophore model **UA2** derived from three closely related rhodanine analogs;[24] green spheres = hydrophobic features; red sphere = anionic feature (visualized in MOE 2010.10).

Table 3. Two Analogs Utilized by Panchal et al.[46] To Derive a LF Pharmacophore Hypothesis Covering the S1–S2 Subsite

Cpd #	Structure	LF K_i (μM)
1	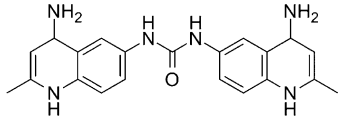	0.50
2	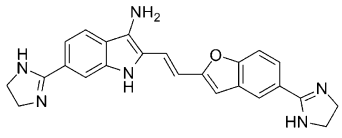	4.90

*Models **UA4** and **UA5:** 1PWQ.pdb (LF Complexed with Thioacetyl-Tyr-Pro-Met-amide) and 1PWU.pdb (LF Bound to Peptide-Based Matrix Metalloprotease Inhibitor **GM6001**).* As no published analogs exist for the small-molecule inhibitors in these two X-ray structures, the 2D ligand–receptor interaction maps generated for both complexes (Figures 7a,b and 8a,b) were used to determine key pharmacophoric features on the ligands. Two hydrogen-bond acceptors, one hydrogen-bond donor, and one hydrophobic group were present in the 1PWQ_ thioacetyl ligand; the corresponding features were combined using MOE 2010.10 to form model **UA4** (Figure 7c). Similarly, model **UA5** (Figure 8c) was constructed by assembling three hydrogen-bond acceptors, one hydrogen-bond donor, and one hydrophobic isopropyl group from **GM6001** cocrystallized with LF in 1PWU. Although developing a pharmacophore model on the basis of a single cocrystallized ligand is a nonstandard approach, the significance testing we conducted (see below) indicated that features in models **UA4** and **UA5** played key roles in identifying potent LF inhibitors, as well as in rejecting weakly potent and inactive compounds.

Comprehensive Pharmacophore Hypothesis: Construction, Validation, and Refinement. All five models **UA1-UA5** were combined in MOE 2010.10 to form an initial comprehensive hypothesis consisting of 19 features. Ten features required refinement due to redundancy: two hydrogen-bond acceptors, one hydrogen-bond donor, and one hydrophobic feature were present in multiple preliminary hypotheses and, upon combination of the five models, appeared as multiple identical features separated by small distances (≤2.11 Å) in the superimposed X-ray structure assembly. Each group of features was therefore merged using MOE 2010.10 into a single representative feature localized on the group center of mass, where the radius of the merged feature was manually adjusted to cover the three-dimensional space occupied by the corresponding feature group. The resulting intermediate model **UM1A** comprising 13 features is depicted in Figure 9.

Subsequent refinement and validation of **UM1A** was done by using that model to virtually screen small-molecule database **DB1** comprising all 546 nonredundant compounds[6,9,14–35] with reported experimental activity data against LF. (Note that compound analogs used to generate the GA-based preliminary models **UA1** and **UA2** had previously been removed from this

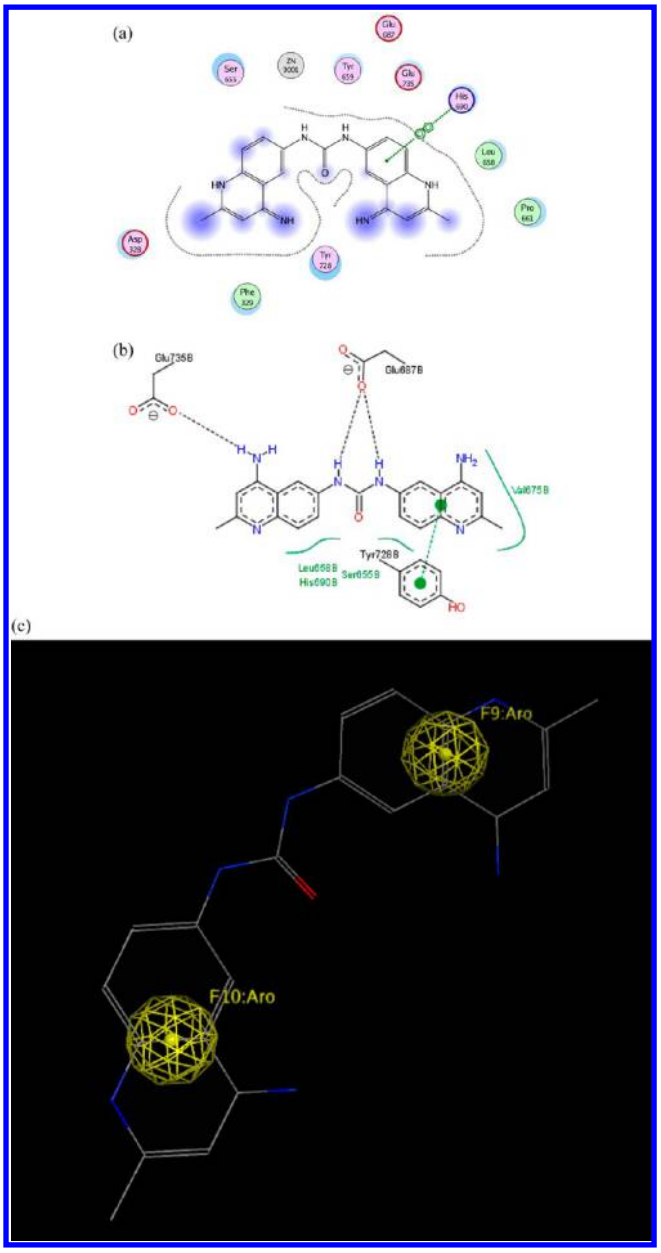

Figure 6. (a) Ligand−receptor interaction diagram of methylquinoline urea compound **NSC 12155** cocrystallized with the anthrax toxin lethal factor (1PWP.pdb[46]) (MOE 2010.10). (b) Additional ligand−receptor interaction map of **NSC 12155** bound to LF (1PWP.pdb[46]) (PoseViewWeb[66]). (c) Preliminary LF inhibitor pharmacophore model **UA3** derived from the published hypothesis of Panchal et al.[46] and modified on the basis of enzyme−inhibitor interactions observed in the 1PWP.pdb X-ray structure; yellow spheres = aromatic centers (visualized in MOE 2010.10).

data set.) Database **DB1** was divided into five initial subsets according to experimental biological activity values (Tables 4 and 5): **DB1A** (strongly active compounds, IC_{50} or K_i < 1 μM, 102 structures); **DB1B** (weakly active compounds, IC_{50} or K_i = 1−100 μM, 320 structures); **DB1C** (inactive compounds with specified biological activity values from dose−response screens, IC_{50} or K_i > 100 μM, 9 structures); **DB1D** (115 compounds for which reported activity values were nonspecific and greater than 25 μM); and **DB1E** (47 compounds in **DB1D** for which reported activity values were nonspecific and greater than 100 μM). For validation purposes, the strongly active compound set

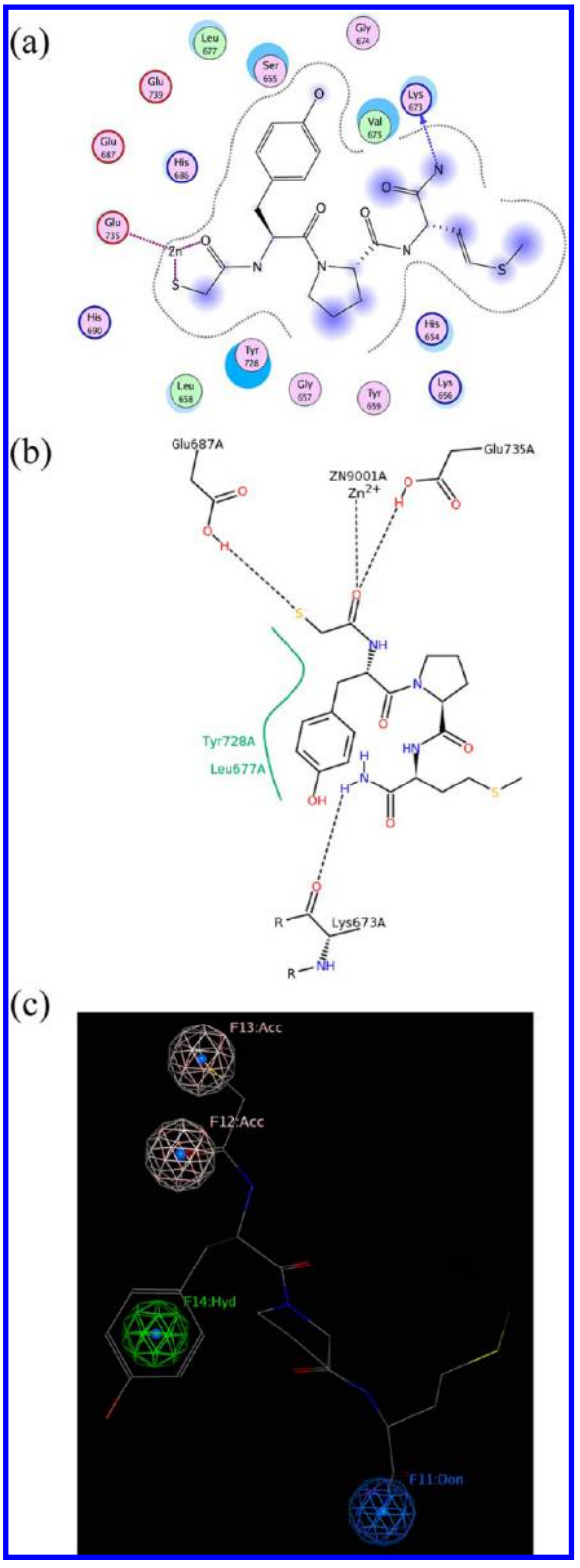

Figure 7. (a) Ligand−receptor interaction diagram of thioacetyl-Tyr-Pro-Met amide cocrystallized with the anthrax toxin lethal factor (1PWQ.pdb[36]) (MOE 2010.10). (b) Additional ligand−receptor interaction map of thioacetyl-Tyr-Pro-Met amide bound to LF (1PWQ.pdb[36]) (PoseViewWeb[66]). (c) Preliminary LF inhibitor pharmacophore model **UA4** developed from the 2D enzyme−inhibitor interaction diagrams; green sphere = hydrophobic center; pink spheres = hydrogen-bond acceptors; blue spheres = hydrogen-bond donors (visualized in MOE 2010.10).

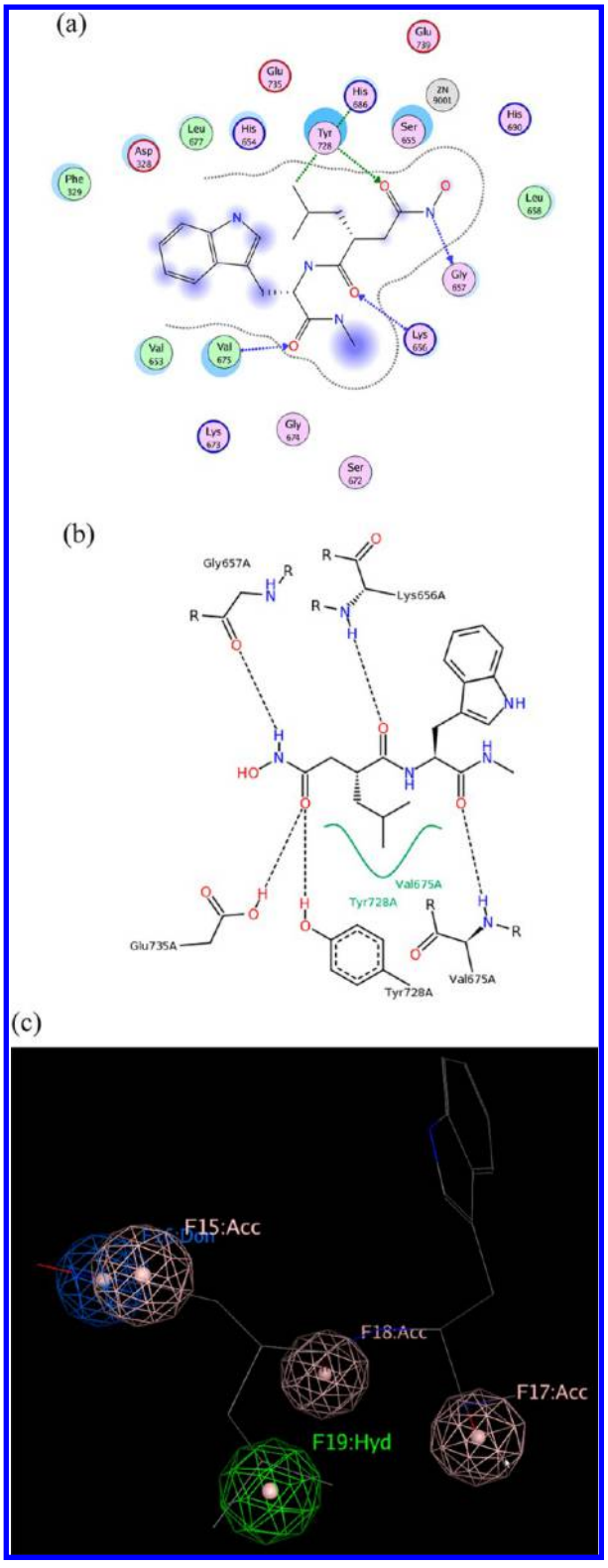

Figure 8. (a) Ligand−receptor interaction diagram of peptidic matrix metalloproteinase inhibitor **GM6001** cocrystallized with the anthrax toxin lethal factor (1PWU.pdb[36]) (MOE 2010.10). (b) Additional ligand−receptor interaction map of **GM6001** complexed with LF (1PWU.pdb[36]) (PoseViewWeb[66]). (c) Preliminary LF inhibitor pharmacophore model **UA5** developed from the 2D enzyme−inhibitor interaction diagrams; green sphere = hydrophobic center; pink spheres = hydrogen-bond acceptors; blue sphere = hydrogen-bond donor (visualized in MOE 2010.10).

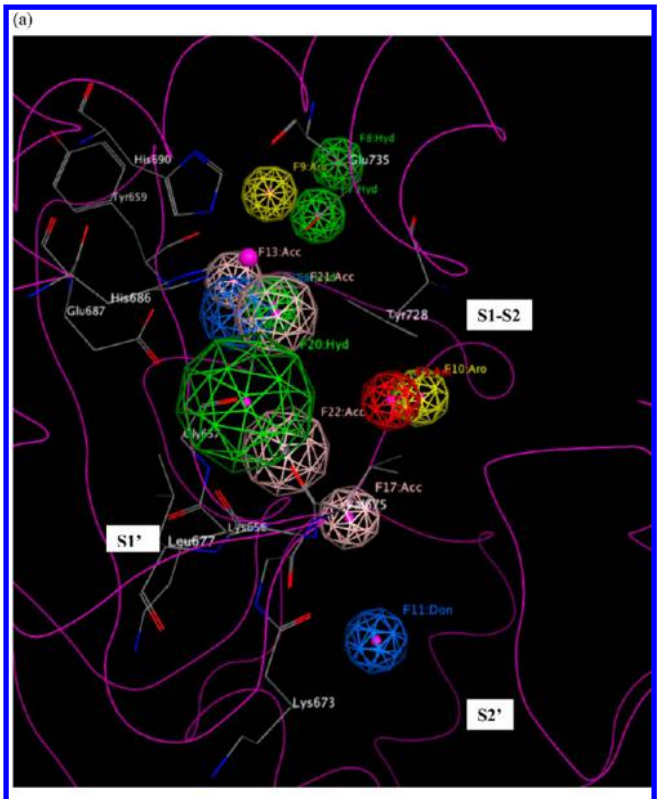

(b)

Feature ID	Feature Type	Radius (Å)
F5	Ani	1.0
F6	Hyd	1.0
F7	Hyd	1.0
F8	Hyd	1.0
F9	Aro	1.0
F10	Aro	1.0
F11	Don	1.0
F13	Acc	1.0
F17	Acc	1.0
F20	Hyd	2.2
F21	Acc	1.4
F22	Acc	1.5
F23	Don	1.3

Figure 9. (a) Intermediate comprehensive LF pharmacophore hypothesis **UM1A,** superimposed on the LF active site (1YQY.pdb[55]),), with key receptor residues, catalytic Zn^{2+} (magenta sphere), and three binding subsites displayed (MOE 2010.10). (b) List of features and their radii in **UM1A:** Don = hydrogen-bond donor; Ani = anion; Hyd = hydrophobic; Aro = aromatic; Acc = hydrogen-bond acceptor.

DB1A was further subdivided into training and test sets: **DB1A_Training** (34 sulfonamide hydroxamate and rhodanine-based derivatives from refs 9, 16, 24, and 26) and **DB1A_Test** (68 compounds from refs 15, 20, 21, 22, 23, 27, 29, and 34 including guanidinylated 2,5-dideoxystreptamine derivatives; guanidinylated derivatives of neamine, aniline, and *γ*-ether derivatives; a carboxylic and *N*-sulfonylated phenylfuran derivative; one *N*-hydroxyhexanamide analog; and (-)-epigallocatechin-3-gallate). The sulfonamide hydroxamate and rhodanine-based **DB1A** compounds were chosen to constitute the training rather than the test set because those structures were similar to those used to construct preliminary pharmacophore hypotheses **UA1** and **UA2**, and for proper model validation, it is important for the test set to be unbiased, i.e., to comprise compounds that had not been used in model

Table 4. Results of Significance Test on Comprehensive LF Pharmacophore Hypothesis UM1A, Illustrating the Number of Compounds in Each Database Subset Returned by the Hypothesis When the Designated Pharmacophoric Feature Was Removed

feature removed	DB1A_Training	DB1B	DB1C	DB1D	DB1E
None (UM1A)	33/34[a]	251/320	4/9	66/115	26/47
F5 Ani[b]	33	251	4/9	66	26
F6 Hyd	25	208	4/9	55	20
F7 Hyd	25	191	4/9	50	18
F8 Hyd	24	221	4/9	57	23
F9 Aro	33	228	4/9	55	21
F10 Aro	33	247	4/9	65	26
F11 Don	33	250	3/9	66	26
F13 Acc	17	212	4/9	54	24
F17 Acc	33	237	4/9	62	26
F20 Hyd	13	159	2/9	32	16
F21 Acc	13	157	3/9	39	19
F22 Acc	17	199	3/9	49	20
F23 Don	17	209	2/9	57	23

[a]Total number of compounds in each database subset. [b]Ani = anion; Hyd = hydrophobic; Aro = aromatic; Don = hydrogen-bond donor; Acc = hydrogen-bond acceptor.

Table 5. Performance of Intermediate Comprehensive Pharmacophore Hypothesis UM1A and Final Comprehensive Hypothesis UM1 As Evaluated by Virtual Screening of Published Active and inactive LF Inhibitors

database subset	experimental activity range of cpds in subset (IC_{50} or K_i values, μM)	# cpds in subset	# of "hits" and % cpds returned by model **UM1A**	# of "hits" and % cpds returned by refined model **UM1**
DB1A_Training	<1	34	33, 97.1%	29, 85.3%
DB1A_Test	<1	68	67, 98.5%	49, 72.1%
DB1B	1−100	320	251, 78.4%	122, 38.1%
DB1C	>100	9	4, 44.4%	0, 0.0%
DB1D	unspecified[a]	115	66, 57.4%	26, 22.6%
DB1E	unspecified[b]	47	26, 55.3%	8, 17.0%

[a]Compounds for which published biological activities were nonspecific, e.g., "greater than 25 micromolar". [b]Compounds for which published biological activities were nonspecific but "greater than 100 micromolar," a subset of **DB1D**.

construction and that are structurally dissimilar to those in the training set.

In the first stage of this virtual screen, a partial-match validation test was done to find the optimal minimum number of pharmacophoric features in **UM1A** that must be matched by a given compound, for that compound to be considered a "hit". Requiring at least four features to be matched resulted in a relatively high hit rate across the entire data set, irrespective of activity: **UM1A** returned all 34 highly active compounds in **DB1A_Training** (LF IC_{50} or K_i less than one micromolar), all of the less actives (**DB1B**), 77.8% of the inactive **DB1C** structures, 95.7% of the inactives in our set with unspecified biological activity values, and 93.6% of those inactives with nonspecific activities reported as greater than 100 μM—meaning that the majority of structures in the 546-compound database matched 4 of the 13 features in **UM1A**, and that a partial match criterion of ≥4 would not be sufficient to distinguish more potent from less potent compounds. Increasing the partial match criterion to ≥5 resulted in 97.1% of highly actives in **DB1A_Training** and 78.4% of the less actives being identified, but requiring at least 6 features to be matched, greatly decreased the active compound hit rate to 2.9% (only one out of 34 structures). Consequently, a partial match criterion of five features was established for subsequent further refinement and screening.

Next, a significance test was conducted on **UM1A** to assess whether each of its 13 features must be present in order for the model to identify active compounds and reject inactives. This was done by removing one feature at a time from the hypothesis (keeping the partial match requirement of at least five features as described above), using the resulting 12-featured model to screen the entire **DB1** test set (MOE 2010.10), and comparing the results to those obtained by using the full 13-featured model (Table 4). The unaltered model **UM1A** returned 33 (97.1%, **DB1A_Training**) highly active compounds in the training set, 67 (98.5%, **DB1A_Test**) highly active compounds in the test set, and 251 of 320 (78.4%) less active compounds (**DB1B**), while rejecting 5 out of 9 (55.5%) inactive compounds (**DB1C**), 49 of 115 (42.6%) nonspecifics (**DB1D**), and 21 of 47 (44.6%) nonspecifics with activities reported as greater than 100 μM. Omitting anionic feature F5 had no effect on hit rate; the effect of removing features F10, F11, and F17 was also negligible (a change of ≤1% "hit" or "match" rate across all four subsets), indicating that none of these features played a significant role in identifying actives and could be safely omitted from the model. Omitting aromatic feature F9 resulted in a model that returned the same numbers of strongly active compounds in the training set (33 of 34) and specified inactives (4 of 9) as did **UM1A** but resulted in an improvement in selectivity, as it matched 16 fewer nonspecifics in data sets **DB1D** and **DB1E**. Subsequently, the radii of the remaining features were optimized to minimize the return rates of inactives and nonspecifics (**DB1C** and **DB1E** compounds) while maintaining a reasonable hit rate for highly active compounds (**DB1A_Training**). On the basis of our significance test results, F20 and F23 played the most significant roles in matching **DB1C** compounds, as removal of either caused the largest decrease in the **DB1C** hit rate (Table 4). The radii of F20 and F23 were therefore reduced by 0.1 Å increments until the **DB1C** hit rate reached zero. The presence of hydrogen-bond acceptor feature F13 strongly influenced the **DB1A_Training** hit rate, so the radius of this feature was increased by 0.1 Å increments until a temporary maximum **DB1A_Training** hit rate was achieved. Next, the radii of all features were fine-tuned until minimal hit rates for **DB1C** and **DB1E** and maximal hit rates for **DB1A_Training** were reached. This final comprehensive model **UM1** is shown in Figure 10. (Note that although feature F13 originated from models **UA4** and **UA5** that were derived using structure-based interaction maps rather than by means of traditional pharmacophore mapping procedures using sets of ligand analogs, our significance test proved that this feature was required in order for the comprehensive model to pinpoint active compounds).

We found that this final hypothesis **UM1** performed quite well in terms of selectively returning strongly active vs less active LF inhibitors (Table 5): 72.1% of the unbiased **DB1A_Test** structures vs 38.1% of **DB1B** structures. **UM1** also strongly disfavored inactive compounds, identifying *none* of the **DB1C** structures and only 22.6% of the structures with "unspecified" activities in **DB1D**—and only 8 of the 47

dx.doi.org/10.1021/ci300121p | J. Chem. Inf. Model. 2012, 52, 1886−1897

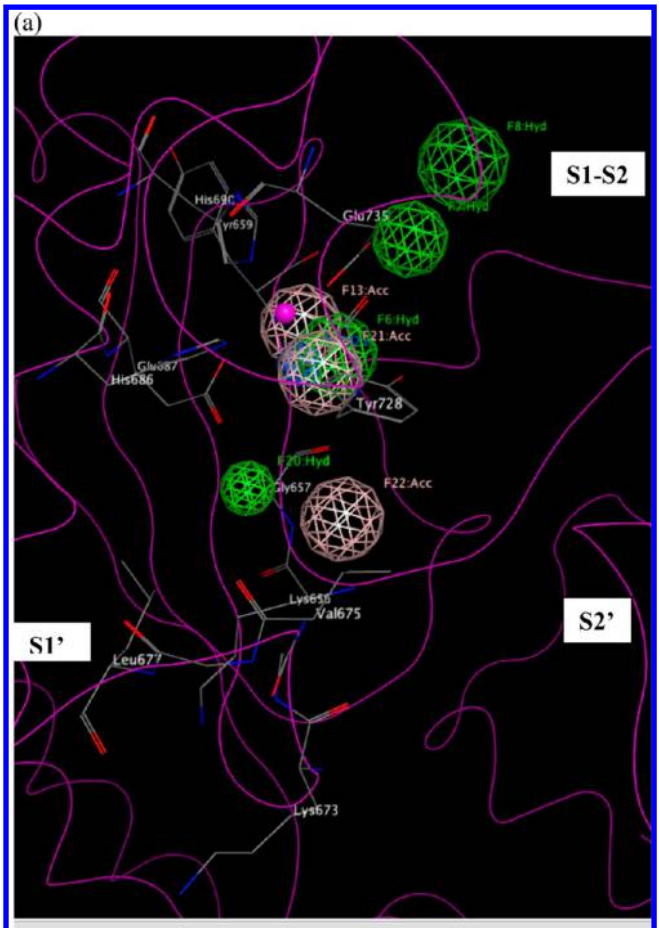

(b)

Feature ID	Feature Type	Radius (Å)
F6	Hyd	1.3
F7	Hyd	1.2
F8	Hyd	1.5
F13	Acc	1.3
F20	Hyd	0.8
F21	Acc	1.3
F22	Acc	1.3
F23	Don	0.7

Figure 10. (a) Final comprehensive LF pharmacophore hypothesis **UM1**, superimposed on the LF active site (1YQY.pdb[55]), with key receptor residues, catalytic Zn^{2+} (magenta sphere), and three binding subsites displayed (MOE 2010.10). (b) List of features and their radii in **UM1**: Hyd = hydrophobic; Acc = hydrogen-bond acceptor; Don = hydrogen-bond donor.

compounds in **DB1E** with "unspecified" activities greater than 100 μM. Note also that while **UM1** identified fewer strongly active compounds in **DB1A_Test** than did **UM1A** (73.5% vs 98.5%), this refined model was able to distinguish more precisely between nanomolar- and micromolar-level compounds, matching only 38.1% vs 78.4% of **DB1B** structures. Importantly, the high selectivity of **UM1** for strong actives was not due to significant structural similarity between compounds used to build/optimize the model and those in the test set; the mean Tanimoto similarity for nearest-neighbor compounds in the training (**DB1A_Training**) and test (**DB1A_Test**) data sets was only 0.51.

Figure 10 illustrates hypothesis **UM1** superimposed on the X-ray structure of the LF active site (1YQY.pdb),[55] with all eight features illustrated: F6–F8, F13, and F20–F23. Hydrophobic features F6–F8, originating from preliminary model **UA2**, represent inhibitor moieties that are necessary to interact with residues in the hydrophobic S1–S2 and zinc-chelating regions of the LF active site. A key hydrogen-bonding interaction with Glu687 near the catalytic Zn^{2+} is represented by feature F13. Other hydrophobic interactions that may enhance compound activity are indicated by feature F20 (with the zinc-binding residue His686, Tyr728 in the LF S1–S2 region, Leu677 in the S1′ subsite, and with Lys656 in the less explored S2′ area). Feature F21 points to key hydrogen-bonding interactions between the ligand with Glu735 and Tyr728 in the S1-S2 area, while F22 represents a hydrogen-bond acceptor that may enhance binding by interacting with Gly657 near the bottom of the active site and Lys656 in the S2′ region. Finally, the donor feature F23 indicates two hydrogen bonds from the ligand to Gly657 and Glu687. Note that hydrophobic and/or hydrogen bonding interactions involving Tyr728, Gly657, and Glu687 are represented by multiple pharmacophoric features in **UM1**, suggesting that these residues may be especially important targets in the LF active site.

Concluding Remarks. In this paper, we have presented a new pharmacophore hypothesis **UM1** for anthrax toxin lethal factor (LF) inhibitors, obtained from experimental X-ray binding modes of structurally diverse active compounds and spanning all three key subsites in the LF binding area. This eight-featured, comprehensive model was constructed from five preliminary models and was validated and optimized by screening all published LF inhibitors with experimental biological activity data—an extremely diverse data set occupying a variety of distinct regions in chemical space—including an unbiased test set of 68 nM-level LF inhibitors that are not structurally related to the compounds used in pharmacophore construction. When applied with a partial match criterion of at least five features, **UM1** successfully identified 72.1% of the LF inhibitors in this test database, i.e., with biological activities less than 1 μM, and returned none of the published compounds with specified activities greater than 100 μM. Key design principles for active LF inhibitors are also illustrated by this pharmacophore hypothesis: for good potency, a small molecule should incorporate hydrophobic moieties to interact with residues in all three subsites including Lys656, Leu677, His686, and Tyr728; a selection of hydrogen-bond acceptors to interact with Glu687, Glu735, Tyr 728, Lys656, and/or Gly657; and a moiety that can function as a hydrogen-bond donor to Gly657 or Glu687. Notably, model **UM1** was derived from experimentally determined bound configurations of a variety of active, structurally diverse LF inhibitors and was validated against an even more diverse LF inhibitor compound database with a broad range of biological activities, including an external test set. Incorporating structural biology data via 2D ligand–receptor interaction maps increased the accuracy and predictability of the final model, and interaction maps for a single ligand and the LF target were able to provide enough information to generate models with essential features (as determined by significance testing) even when a series of active analogs was not available for traditional pharmacophore perception methods. We therefore recommend

final model **UM1** as an in silico searching tool to rapidly screen compound collections for new potential LF inhibitor scaffolds. Because this model additionally points to critical ligand–receptor interactions present in multiple X-ray structures of LF cocrystallized with small molecules (some of which were also revealed by genetic algorithm-based pharmacophore perception methodologies), we also recommend **UM1** as an adjunct tool in lead optimization to help increase the potency of existing compounds.

METHODS AND COMPUTATIONAL DETAILS

X-ray Structure Preparation. In order to obtain a structural superimposition for pharmacophore perception, the five LF-inhibitor crystal structures available in the Protein Data Bank (1YQY,[55] 1ZXV,[16] 1PWP,[46] 1PWU,[36] and 1PWQ[36]) were aligned in Cartesian space by optimizing the sum of all pairwise alignment scores using the Homology/Align module in MOE 2010.10 (Chemical Computing Group, Inc.), with alignment based on protein coordinates rather than cocrystallized ligand coordinates.

Preparation of Small Molecules for Pharmacophore Perception. For the genetic algorithm-based models **UA1** and **UA2**, all analogs used to construct models were built from the respective cocrystallized ligands (**LF-1B** in the case of **UA1** and **BI-MFM3** in the case of **UA2**). Each analog was then subjected to geometry optimization within the respective enzyme active site (X-ray structural coordinates) in order to approach a putative bound conformation as closely as possible. Minimization was done in MOE 2010.10 using the MMFF94s force field[68,69] with a convergence criterion of 0.05 kcal/mol·Å, while the receptor was held rigid.

Screening Data set Preparation. A database of 546 nonredundant LF inhibitors (**DB1**) was assembled from structural and biological activity data reported in a total of 23 published works.[6,9,14−31,33−35] Each compound was individually sketched in MOE 2010.10 (Chemical Computing Group, Inc.) and was geometry optimized using the MMFF94s force field,[68,69] applying a convergence criterion of 0.05 kcal/mol·Å. **DB1** was divided into six total subsets, including training and test sets for nanomolar-level compounds, as described earlier. To obtain predicted bound conformations of these structures, each minimized compound was then docked into the LF active site (1YQY.pdb[55]) using Surflex-Dock[70−73] and the CScore consensus scoring module[74] in the SYBYL 8.0 discovery software suite (Tripos, Inc.). In the docking procedure, the active-site representation (protomol) was defined to encompass all receptor areas that were demonstrated in the X-ray structures to interact with moieties on all five cocrystallized ligands. The docking threshold and bloat parameters were set to 0.5 and 0, respectively. The maximum number of conformations per compound fragment and the maximum number of poses per ligand were both set to 20, and the maximum allowable number of rotatable bonds per molecule was limited to 100. Postdock geometry optimizations were done on each molecule to fine-tune the predicted bound conformations. Tanimoto coefficients measuring similarity between nearest-neighbor training and test set compounds were calculated in Pipeline Pilot 8.0 (Accelrys, Inc.), using ECFP_4 descriptors (Extended-Connectivity Fingerprint with maximum diameter of circular neighborhoods considered for each atom set to 4).

ASSOCIATED CONTENT

Supporting Information

Structures of all 546 published LF inhibitors comprising screening data set **DB1**, divided into five subsets according to biological acitivity (with **DB1A** training and test set compounds indicated) and a list of features and pairwise distances for the final revised hypothesis **UM1**. This material is available free of charge via the Internet at http://pubs.acs.org.

AUTHOR INFORMATION

Corresponding Author

*E-mail: eamin@umn.edu.

Notes

The authors declare no competing financial interest.

ACKNOWLEDGMENTS

The authors express their gratitude to Barry Finzel, Todd Geders, and Michael Walters for helpful discussions, and to the reviewers of this work for valuable observations and suggestions. This study was supported in part by the University of Minnesota Supercomputing Institute for Advanced Computational Research, and by the National Institutes of Health (R01 AI083234 to E.A.A.).

REFERENCES

(1) Pezard, C.; Berche, P.; Mock, M. Contribution of individual toxin components to virulence of Bacillus anthracis. *Infect. Immun.* **1991**, *59*, 3472−3477.

(2) Chopra, A. P.; Boone, S. A.; Liang, X.; Duesbery, N. S. Anthrax lethal factor proteolysis and inactivation of MAPK kinase. *J. Biol. Chem.* **2003**, *278*, 9402−9406.

(3) Bardwell, A. J.; Abdollahi, M.; Bardwell, L. Anthrax lethal factor-cleavage products of MAPK (mitogen-activated protein kinase) kinases exhibit reduced binding to their cognate MAPKs. *Biochem. J.* **2004**, *378*, 569−577.

(4) Tanoue, T.; Nishida, E. Molecular recognitions in the MAP kinase cascades. *Cell. Signal.* **2003**, *15*, 455−462.

(5) Biondi, R. M.; Nebreda, A. R. Signalling specificity of Ser/Thr protein kinases through docking-site-mediated interactions. *Biochem. J.* **2003**, *372*, 1−13.

(6) Gaddis, B. D.; Avramova, L. V.; Chmielewski, J. Inhibitors of anthrax lethal factor. *Bioorg. Med. Chem. Lett.* **2007**, *17*, 4575−4578.

(7) Warfel, J. M.; Steele, A. D.; D'Agnillo, F. Anthrax lethal toxin induces endothelial barrier dysfunction. *Am. J. Pathol.* **2005**, *166*, 1871−1881.

(8) Moayeri, M.; Leppla, S. H. The roles of anthrax toxin in pathogenesis. *Curr. Opin. Microbiol.* **2004**, *7*, 19−24.

(9) Xiong, Y.; Wiltsie, J.; Woods, A.; Guo, J.; Pivnichny, J. V.; Tang, W.; Bansal, A.; Cummings, R. T.; Cunningham, B. R.; Friedlander, A. M.; Douglas, C. M.; Salowe, S. P.; Zaller, D. M.; Scolnick, E. M.; Schmatz, D. M.; Bartizal, K.; Hermes, J. D.; MacCoss, M.; Chapman, K. T. The discovery of a potent and selective lethal factor inhibitor for adjunct therapy of anthrax infection. *Bioorg. Med. Chem. Lett.* **2006**, *16*, 964−968.

(10) Turk, B. E. Discovery and development of anthrax lethal factor metalloproteinase inhibitors. *Curr. Pharm. Biotechnol.* **2008**, *9*, 24−33.

(11) Beers, M. H.; Porter, R. S.; Jones, T. V., *The Merck Manual of Diagnosis and Therapy.*, 18th ed.; John Wiley & Sons, Inc.: Hoboken, NJ, 2006.

(12) Guarner, J.; Jernigan, J. A.; Shieh, W. J.; Tatti, K.; Flannagan, L. M.; Stephens, D. S.; Popovic, T.; Ashford, D. A.; Perkins, B. A.; Zaki, S. R. Pathology and pathogenesis of bioterrorism-related inhalational anthrax. *Am. J. Pathol.* **2003**, *163*, 701−709.

(13) Holty, J. E.; Bravata, D. M.; Liu, H.; Olshen, R. A.; McDonald, K. M.; Owens, D. K. Systematic review: A century of inhalational

anthrax cases from 1900 to 2005. *Ann. Intern. Med.* **2006**, *144*, 270−280.
(14) Agrawal, A.; Johnson, S. L.; Jacobsen, J. A.; Miller, M. T.; Chen, L. H.; Pellecchia, M.; Cohen, S. M. Chelator fragment libraries for targeting metalloproteinases. *ChemMedChem* **2010**, *5*, 195−199.
(15) Dell'Aica, I.; Dona, M.; Tonello, F.; Piris, A.; Mock, M.; Montecucco, C.; Garbisa, S. Potent inhibitors of anthrax lethal factor from green tea. *EMBO Rep.* **2004**, *5*, 418−422.
(16) Forino, M.; Johnson, S.; Wong, T. Y.; Rozanov, D. V.; Savinov, A. Y.; Li, W.; Fattorusso, R.; Becattini, B.; Orry, A. J.; Jung, D.; Abagyan, R. A.; Smith, J. W.; Alibek, K.; Liddington, R. C.; Strongin, A. Y.; Pellecchia, M. Efficient synthetic inhibitors of anthrax lethal factor. *Proc. Natl. Acad. Sci. U.S.A.* **2005**, *102*, 9499−9504.
(17) Gaddis, B. D.; Rubert Perez, C. M.; Chmielewski, J. Inhibitors of anthrax lethal factor based upon N-oleoyldopamine. *Bioorg. Med. Chem. Lett.* **2008**, *18*, 2467−2470.
(18) Hanna, M. L.; Tarasow, T. M.; Perkins, J. Mechanistic differences between in vitro assays for hydrazone-based small molecule inhibitors of anthrax lethal factor. *Bioorg. Chem.* **2007**, *35*, 50−58.
(19) Jacobsen, J. A.; Fullagar, J. L.; Miller, M. T.; Cohen, S. M. Identifying chelators for metalloprotein inhibitors using a fragment-based approach. *J. Med. Chem.* **2011**, *54*, 591−602.
(20) Jiao, G. S.; Cregar, L.; Goldman, M. E.; Millis, S. Z.; Tang, C. Guanidinylated 2,5-dideoxystreptamine derivatives as anthrax lethal factor inhibitors. *Bioorg. Med. Chem. Lett.* **2006**, *16*, 1527−1531.
(21) Jiao, G. S.; Simo, O.; Nagata, M.; O'Malley, S.; Hemscheidt, T.; Cregar, L.; Millis, S. Z.; Goldman, M. E.; Tang, C. Selectively guanidinylated derivatives of neamine. Syntheses and inhibition of anthrax lethal factor protease. *Bioorg. Med. Chem. Lett.* **2006**, *16*, 5183−5189.
(22) Jiao, G. S.; Cregar, L.; Wang, J.; Millis, S. Z.; Tang, C.; O'Malley, S.; Johnson, A. T.; Sareth, S.; Larson, J.; Thomas, G. Synthetic small molecule furin inhibitors derived from 2,5-dideoxystreptamine. *Proc. Natl. Acad. Sci. U.S.A.* **2006**, *103*, 19707−19712.
(23) Jiao, G. S.; Kim, S.; Moayeri, M.; Cregar-Hernandez, L.; McKasson, L.; Margosiak, S. A.; Leppla, S. H.; Johnson, A. T. Antidotes to anthrax lethal factor intoxication. Part 1: Discovery of potent lethal factor inhibitors with in vivo efficacy. *Bioorg. Med. Chem. Lett.* **2010**, *20*, 6850−6853.
(24) Johnson, S. L.; Jung, D.; Forino, M.; Chen, Y.; Satterthwait, A.; Rozanov, D. V.; Strongin, A. Y.; Pellecchia, M. Anthrax lethal factor protease inhibitors: Synthesis, SAR, and structure-based 3D QSAR studies. *J. Med. Chem.* **2006**, *49*, 27−30.
(25) Johnson, S. L.; Chen, L. H.; Pellecchia, M. A high-throughput screening approach to anthrax lethal factor inhibition. *Bioorg. Chem.* **2007**, *35*, 306−312.
(26) Johnson, S. L.; Chen, L. H.; Harbach, R.; Sabet, M.; Savinov, A.; Cotton, N. J.; Strongin, A.; Guiney, D.; Pellecchia, M. Rhodanine derivatives as selective protease inhibitors against bacterial toxins. *Chem. Biol. Drug Des.* **2008**, *71*, 131−139.
(27) Johnson, S.; Barile, E.; Farina, B.; Purves, A.; Wei, J.; Chen, L. H.; Shiryaev, S.; Zhang, Z.; Rodionova, I.; Agrawal, A.; Cohen, S. M.; Osterman, A.; Strongin, A.; Pellecchia, M. Targeting metalloproteins by fragment-based lead discovery. *Chem. Biol. Drug Des.* **2011**, *78*, 211−223.
(28) Johnson, S. L.; Chen, L. H.; Barile, E.; Emdadi, A.; Sabet, M.; Yuan, H.; Wei, J.; Guiney, D.; Pellecchia, M. Structure−activity relationship studies of a novel series of anthrax lethal factor inhibitors. *Bioorg. Med. Chem.* **2009**, *17*, 3352−3368.
(29) Kim, S.; Jiao, G. S.; Moayeri, M.; Crown, D.; Cregar-Hernandez, L.; McKasson, L.; Margosiak, S. A.; Leppla, S. H.; Johnson, A. T. Antidotes to anthrax lethal factor intoxication. Part 2: Structural modifications leading to improved in vivo efficacy. *Bioorg. Med. Chem. Lett.* **2011**, *21*, 2030−2033.
(30) Lewis, J. A.; Mongan, J.; McCammon, J. A.; Cohen, S. M. Evaluation and binding-mode prediction of thiopyrone-based inhibitors of anthrax lethal factor. *ChemMedChem* **2006**, *1*, 694−697.
(31) Li, B.; Pai, R.; Cardinale, S. C.; Butler, M. M.; Peet, N. P.; Moir, D. T.; Bavari, S.; Bowlin, T. L. Synthesis and biological evaluation of botulinum neurotoxin a protease inhibitors. *J. Med. Chem.* **2010**, *53*, 2264−2276.
(32) Min, D. H.; Tang, W. J.; Mrksich, M. Chemical screening by mass spectrometry to identify inhibitors of anthrax lethal factor. *Nat. Biotechnol.* **2004**, *22*, 717−723.
(33) Numa, M. M.; Lee, L. V.; Hsu, C. C.; Bower, K. E.; Wong, C. H. Identification of novel anthrax lethal factor inhibitors generated by combinatorial Pictet-Spengler reaction followed by screening in situ. *ChemBioChem* **2005**, *6*, 1002−1006.
(34) Schepetkin, I. A.; Khlebnikov, A. I.; Kirpotina, L. N.; Quinn, M. T. Novel small-molecule inhibitors of anthrax lethal factor identified by high-throughput screening. *J. Med. Chem.* **2006**, *49*, 5232−5244.
(35) Yuan, H.; Johnson, S. L.; Chen, L. H.; Wei, J.; Pellecchia, M. A novel pharmacophore model for the design of anthrax lethal factor inhibitors. *Chem. Biol. Drug Des.* **2010**, *76*, 263−268.
(36) Turk, B. E.; Wong, T. Y.; Schwarzenbacher, R.; Jarrell, E. T.; Leppla, S. H.; Collier, R. J.; Liddington, R. C.; Cantley, L. C. The structural basis for substrate and inhibitor selectivity of the anthrax lethal factor. *Nat. Struct. Mol. Biol.* **2004**, *11*, 60−66.
(37) Li, F.; Chvyrkova, I.; Terzyan, S.; Wakeham, N.; Turner, R.; Ghosh, A. K.; Zhang, X. C.; Tang, J. Inhibition of anthrax lethal factor: Lability of hydroxamate as a chelating group. *Appl. Microbiol. Biotechnol.* **2012**, *94*, 1041−1049.
(38) Li, F.; Terzyan, S.; Tang, J. Subsite specificity of anthrax lethal factor and its implications for inhibitor development. *Biochem. Biophys. Res. Commun.* **2011**, *407*, 400−405.
(39) Dalkas, G. A.; Chasapis, C. T.; Gkazonis, P. V.; Bentrop, D.; Spyroulias, G. A. Conformational dynamics of the anthrax lethal factor catalytic center. *Biochemistry 49*, 10767-10769.
(40) Roy, J.; Kumar, U. C.; Machiraju, P. K.; Muttineni, R. K.; Kumar, B. V. S. S.; Gundla, R.; Dayam, R.; Sarma, J. A. Insilico studies on anthrax lethal factor inhibitors: Pharmacophore modeling and virtual screening approaches towards designing of novel inhibitors for a killer. *J. Mol. Graph. Model. 29*, 256-265.
(41) Jacobsen, F. E.; Lewis, J. A.; Cohen, S. M. The design of inhibitors for medicinally relevant metalloproteins. *ChemMedChem* **2007**, *2*, 152−171.
(42) Tonello, F.; Seveso, M.; Marin, O.; Mock, M.; Montecucco, C. Screening inhibitors of anthrax lethal factor. *Nature* **2002**, *418*, 386.
(43) Whittaker, M.; Floyd, C. D.; Brown, P.; Gearing, A. J. Design and therapeutic application of matrix metalloproteinase inhibitors. *Chem. Rev.* **1999**, *99*, 2735−2776.
(44) Goldman, M. E.; Cregar, L.; Nguyen, D.; Simo, O.; O'Malley, S.; Humphreys, T. Cationic polyamines inhibit anthrax lethal factor protease. *BMC Pharmacol.* **2006**, *6*, 8.
(45) Karginov, V. A.; Nestorovich, E. M.; Moayeri, M.; Leppla, S. H.; Bezrukov, S. M. Blocking anthrax lethal toxin at the protective antigen channel by using structure-inspired drug design. *Proc. Natl. Acad. Sci. U.S.A.* **2005**, *102*, 15075−15080.
(46) Panchal, R. G.; Hermone, A. R.; Nguyen, T. L.; Wong, T. Y.; Schwarzenbacher, R.; Schmidt, J.; Lane, D.; McGrath, C.; Turk, B. E.; Burnett, J.; Aman, M. J.; Little, S.; Sausville, E. A.; Zaharevitz, D. W.; Cantley, L. C.; Liddington, R. C.; Gussio, R.; Bavari, S. Identification of small molecule inhibitors of anthrax lethal factor. *Nat. Struct. Mol. Biol.* **2004**, *11*, 67−72.
(47) Lee, L. V.; Bower, K. E.; Liang, F. S.; Shi, J.; Wu, D.; Sucheck, S. J.; Vogt, P. K.; Wong, C. H. Inhibition of the proteolytic activity of anthrax lethal factor by aminoglycosides. *J. Am. Chem. Soc.* **2004**, *126*, 4774−4775.
(48) Kocer, S. S.; Walker, S. G.; Zerler, B.; Golub, L. M.; Simon, S. R. Metalloproteinase inhibitors, nonantimicrobial chemically modified tetracyclines, and ilomastat block Bacillus anthracis lethal factor activity in viable cells. *Infect. Immun.* **2005**, *73*, 7548−7557.
(49) Houseman, B. T.; Huh, J. H.; Kron, S. J.; Mrksich, M. Peptide chips for the quantitative evaluation of protein kinase activity. *Nat. Biotechnol.* **2002**, *20*, 270−274.
(50) Min, D. H.; Su, J.; Mrksich, M. Profiling kinase activities by using a peptide chip and mass spectrometry. *Angew. Chem., Int. Ed. Engl.* **2004**, *43*, 5973−5977.

(51) Su, J.; Mrksich, M. Using mass spectrometry to characterize self-assembled monolayers presenting peptides, proteins, and carbohydrates. *Angew. Chem., Int. Ed. Engl.* **2002**, *41*, 4715−4718.
(52) Kim, C.; Gajendran, N.; Mittrucker, H. W.; Weiwad, M.; Song, Y. H.; Hurwitz, R.; Wilmanns, M.; Fischer, G.; Kaufmann, S. H. Human alpha-defensins neutralize anthrax lethal toxin and protect against its fatal consequences. *Proc. Natl. Acad. Sci. U.S.A.* **2005**, *102*, 4830−4835.
(53) Dalkas, G. A.; Papakyriakou, A.; Vlamis-Gardikas, A.; Spyroulias, G. A. Low molecular weight inhibitors of the protease anthrax lethal factor. *Mini. Rev. Med. Chem.* **2008**, *8*, 290−306.
(54) Agrawal, A.; de Oliveira, C. A.; Cheng, Y.; Jacobsen, J. A.; McCammon, J. A.; Cohen, S. M. Thioamide hydroxypyrothiones supersede amide hydroxypyrothiones in potency against anthrax lethal factor. *J. Med. Chem.* **2009**, *52*, 1063−1074.
(55) Shoop, W. L.; Xiong, Y.; Wiltsie, J.; Woods, A.; Guo, J.; Pivnichny, J. V.; Felcetto, T.; Michael, B. F.; Bansal, A.; Cummings, R. T.; Cunningham, B. R.; Friedlander, A. M.; Douglas, C. M.; Patel, S. B.; Wisniewski, D.; Scapin, G.; Salowe, S. P.; Zaller, D. M.; Chapman, K. T.; Scolnick, E. M.; Schmatz, D. M.; Bartizal, K.; MacCoss, M.; Hermes, J. D. Anthrax lethal factor inhibition. *Proc. Natl. Acad. Sci. U.S.A.* **2005**, *102*, 7958−7963.
(56) Chiu, T. L.; Solberg, J.; Patil, S.; Geders, T. W.; Zhang, X.; Rangarajan, S.; Francis, R.; Finzel, B. C.; Walters, M. A.; Hook, D. J.; Amin, E. A. Identification of novel non-hydroxamate anthrax toxin lethal factor inhibitors by topomeric searching, docking and scoring, and in vitro screening. *J. Chem. Inf. Model.* **2009**, *49*, 2726−2734.
(57) Guner, O. F. Pharmacophore modeling in drug design: Recent advances. *Curr. Comput.-Aided Drug Des. 7*, 158.
(58) Khedkar, S. A.; Malde, A. K.; Coutinho, E. C.; Srivastava, S. Pharmacophore modeling in drug discovery and development: An overview. *Med. Chem.* **2007**, *3*, 187−197.
(59) Yang, S. Y. Pharmacophore modeling and applications in drug discovery: Challenges and recent advances. *Drug Discovery Today* **2010**, *15*, 444−450.
(60) Roy, J.; Kumar, U. C.; Machiraju, P. K.; Muttineni, R. K.; Kumar, B. V. S. S.; Gundla, R.; Dayam, R.; Sarma, J. A. In silico studies on anthrax lethal factor inhibitors: Pharmacophore modeling and virtual screening approaches towards designing of novel inhibitors for a killer. *J. Mol. Graph. Model.* **2010**, *29*, 256−265.
(61) Richmond, N. J.; Abrams, C. A.; Wolohan, P. R.; Abrahamian, E.; Willett, P.; Clark, R. D. GALAHAD: 1. Pharmacophore identification by hypermolecular alignment of ligands in 3D. *J. Comput.-Aided Mol. Des.* **2006**, *20*, 567−587.
(62) Cottrell, S. J.; Gillet, V. J.; Taylor, R.; Wilton, D. J. Generation of multiple pharmacophore hypotheses using multiobjective optimization techniques. *J. Comput-Aided Mol. Des.* **2004**, *18*, 665−682.
(63) Gillet, V. J.; Willett, P.; Fleming, P. J.; Green, D. V. Designing focused libraries using MoSELECT. *J. Mol. Graph. Model.* **2002**, *20*, 491−498.
(64) Berman, H. M.; Westbrook, J.; Feng, Z.; Gilliland, G.; Bhat, T. N.; Weissig, H.; Shindyalov, I. N.; Bourne, P. E. The Protein Data Bank. *Nucleic Acids Res.* **2000**, *28*, 235−242.
(65) *GALAHAD Manual, SYBYL 8.0*; Tripos, Inc.: St. Louis, MO, 2007; pp17, 70−71.
(66) Stierand, K.; Maaβ, P., C.; Rarey, M. Molecular complexes at a glance: automated generation of two-dimensional complex diagrams. *Bioinformatics* **2006**, *22*, 1710−1716.
(67) Brickmann, J.; Exner, T. E.; Keil, M.; Marhöfer, R. J. Molecular Graphics - Trends and Perspectives. *J. Mol. Model.* **2000**, *6*, 328−340.
(68) Halgren, T. A. MMFF VII. Characterization of MMFF94, MMFF94s, and other widely available force fields for conformational energies and for intermolecular-interaction energies and geometries. *J. Comput. Chem.* **1999**, *20*, 730−748.
(69) Halgren, T. A. MMFF VI. MMFF94s option for energy minimization studies. *J. Comput. Chem.* **1999**, *20*, 720−729.
(70) Jain, A. N. Surflex: Fully automatic flexible molecular docking using a molecular similarity-based search engine. *J. Med. Chem.* **2003**, *46*, 499−511.
(71) Jain, A. N. Virtual screening in lead discovery and optimization. *Curr. Opin. Drug Discovery Dev.* **2004**, *7*, 396−403.
(72) Jain, A. N. Surflex-Dock 2.1: Robust performance from ligand energetic modeling, ring flexibility, and knowledge-based search. *J. Comput.-Aided Mol. Des.* **2007**, *21*, 281−306.
(73) Pham, T. A.; Jain, A. N. Parameter estimation for scoring protein−ligand interactions using negative training data. *J. Med. Chem.* **2006**, *49*, 5856−5868.
(74) Meng, C. S., B.; Kuntz, I. Automated docking with grid-based energy evaluation. *J. Comput. Chem.* **1992**, *13*, 505−524.